J. Biophotonics **4**, No. 11–12, 788–804 (2011) / **DOI** 10.1002/jbio.201100026

Journal of BIOPHOTONICS

FULL ARTICLE

Quantitative remineralization evolution kinetics of artificially demineralized human enamel using photothermal radiometry and modulated luminescence

Adam Hellen[1,2], *Andreas Mandelis*[*,1,3,4], *Yoav Finer*[2] *and Bennett T. Amaechi*[5]

[1] Center for Advanced Diffusion-Wave Technologies, Department of Mechanical and Industrial Engineering, University of Toronto, 5 King's College Road, Toronto, ON, M5S 3G8, Canada
[2] Faculty of Dentistry, University of Toronto, 124 Edward Street, Toronto, ON, M5G 1G6, Canada
[3] Institute of Biomaterials and Biomedical Engineering, University of Toronto, 164 College Street, Toronto, ON, M5S 3G9, Canada
[4] Quantum Dental Technologies, 748 Briar Hill Avenue, Toronto, ON, M6B 1L3, Canada
[5] Department of Community Dentistry, University of Texas Health Science Center at San Antonio, 7703 Floyd Curl Drive, San Antonio, TX 78229-3900, USA

Received 25 March 2011, revised 16 May 2011, accepted 3 June 2011
Published online 15 July 2011

Key words: demineralization, remineralization, enamel, evolution, kinetics, quantitative, photothermal radiometry, modulated luminescence.

Human molars were subjected to demineralization in acid gel followed by incubation in remineralization solutions without or with fluoride (1 or 1000 ppm). Photothermal radiometry (PTR) and modulated luminescence (LUM) frequency scans were performed prior to and during de/remineralization treatments. Transverse Micro-Radiography (TMR) analysis followed at treatment conclusion to determine mineral loss and lesion depth. The remineralization process illustrated a complex interplay between surface and subsurface mineral deposition, confining the thermal-wave centroid toward the dominating layer. Experimental amplitudes and phases were fitted to a coupled diffuse-photon-density-wave and thermal-wave theoretical model used to quantitatively evaluate evolving changes in thermal and optical properties of de/remineralized enamel lesions. Additional information obtained from the LUM data corroborated the remineralization kinetics affecting the PTR signals. The results pointed to enhanced effectiveness of subsurface lesion remineralization in the presence of fluoride.

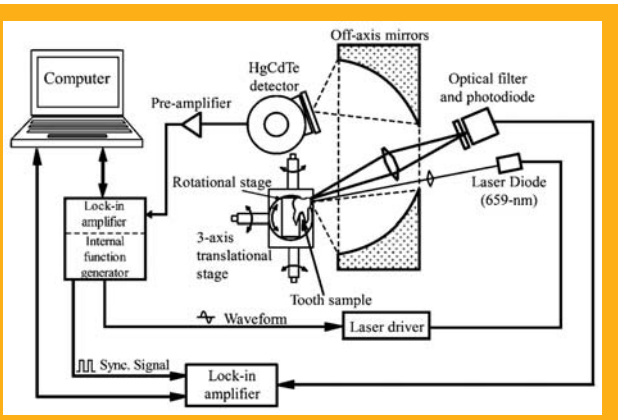

Schematic of the PTR-LUM experimental set-up.

* Corresponding author: e-mail: mandelis@mie.utoronto.ca, Tel./Fax: +1 416 978 5106

1. Introduction

With the recent advancement in techniques available for caries detection, incipient lesions can be detected and their progression monitored non-invasively and non-destructively, while at the same time avoiding continual exposure to harmful ionizing radiation. Acquiring the ability to monitor the progression of incipient lesions over time is an important parameter as part of a clinician's diagnostic arsenal. This will allow the clinician to ultimately determine whether lesions progress to the point where therapeutic agents might be encouraged to reverse and/or arrest the non-cavitated lesion or to the point of cavitation where restorative intervention is necessary.

The process of mineral recovery to repair initial carious lesions involves the passive transport of salivary or plaque calcium and phosphate ions, at neutral pH, down their concentration gradients into the lesion body [1]. As the remineralization process *in vivo* takes considerable amount of time, a multitude of studies have investigated ways to enhance this process, the most well-documented being the incorporation of fluoride and its effects on inhibiting demineralization and enhancing remineralization. Soluble calcium phosphate phases are transformed to a more stable and less acid soluble phase, in the presence of fluoride, through the precipitation of fluorapatite (FAP) or fluoridated hydroxyapatite (F-OHAp) on existing demineralized crystallites or through the nucleation of new crystallites. The mechanism of fluoride incorporation as FAP concomitant with its strong affinity for calcium ions has been the basis for numerous *in vitro* and *in vivo* studies demonstrating enhanced remineralization, particularly in the presence of low fluoride (typically ≤ 1 ppm) concentrations in solution [2].

Although intuitively mineral reintroduction into porous demineralized enamel from saliva or plaque appears simple, the process does not proceed without its challenges. One challenge relates to the limitation of remineralization due to reduced ion diffusion fluxes from the external solution [2]. With excessive fluoride concentrations and/or large solution supersaturation conditions with respect to enamel, rapid mineral deposition may occur preferentially within the enamel surface layer and obstruct surface enamel porosities leading to a disconnect between the external environment (saliva and plaque fluid) and the internal environment (subsurface lesion body). Thus, the deposition of mineral at a particular depth within a carious lesion depends on both the local availability of partially demineralized crystallites, which act as mineral scaffolds, as well as the local supersaturation, fluoride levels and pH [2].

A common challenge in caries research is evaluating the efficacy and effectiveness of remineralization of initial carious lesions. Clinically, remineralized lesions are evaluated using subjective signals such as visual and tactile examination, which are limited to the lesion surface. Furthermore, *in vitro*, multiple thin sections are often implemented to measure changes before and after remineralization, however, the results cannot be directly extrapolated to the clinical reality. Given the advancement in caries detection systems, evaluating depth-resolved changes in mineralization in intact whole teeth, non-destructively, is possible, using substrates more reflective of those in the oral environment. Instruments based on optical fluorescence, for example, Quantitative Light-induced Fluorescence (QLF^{TM}), capture images of a tooth by illuminating with blue-violet light, and have demonstrated efficacy as a tool to detect and longitudinally monitor the progression of artificial caries-like lesions and their subsequent remineralization [3]. Another optical imaging device, polarization-sensitive optical coherence tomography (PS-OCT), based upon light interference within teeth following illumination at near-IR wavelengths, has demonstrated its ability to image demineralized and fluoride-enhanced remineralized artificial lesions [4].

The majority of early detection technologies, including the two aforementioned techniques, are based on the unique optical properties of teeth. When a light source strikes a tooth, the light distribution and energy propagation can be characterized by measuring the light scattering (μ_s) and absorption coefficients (μ_a), which refer to the average number of absorption and scattering events per unit length of a photon propagating through a medium [5]. As most laser-tissue interactions are thermal in nature, the optical-to-thermal energy conversion reactions following photon absorption and the subsequent non-radiative heat conversion, propagation/decay and tissue responses are important physical parameters to consider. Thermal parameters include thermal diffusivity (α) and thermal conductivity (κ), which refer to the rate and amount of heat diffusion through a medium, respectively.

Photothermal radiometry (PTR) is a novel methodology for the characterization of early carious lesions [6]. The basis of photothermal radiometry relies on the conversion of absorbed optical energy into thermal energy, and the subsequent observation of modulated mid-infrared emission. A periodic heat source, such as an intensity modulated laser beam, results in the generation of a periodic temperature distribution within a material. This oscillatory temperature field arising within each light-absorbing layer of a material launches temperature waves known as 'thermal waves' which rapidly decay over the sample depth. The deeper penetration of the thermal field compared to the purely optical field underscores the sensitivity of photothermal techniques to the inspection of optically opaque or scattering materials well beyond the range of optical imaging devices. The induced rise in

temperature results in the generation of thermal infrared photons which can propagate outward to the surrounding medium by virtue of IR spectral transparencies ("windows") of the enamel and be captured by suitable IR detectors. As a complementary signal channel to PTR, modulated luminescence (LUM) monitors the optical-to-radiative energy conversion, where photon absorption and excitation to a higher-energy state is followed by de-excitation to a lower energy state and emission of longer wavelength photons. As a purely optical technique, the higher scattering coefficients of enamel and dentin significantly limit LUM optical penetration depths.

The detection of thermal waves from sound and incipient carious lesions has been accompanied by a concomitant comprehensive theoretical description of the generated thermal-wave signal inside a sample. This has led to the development and application of a robust and complex fitting algorithm for the generation of independent sets and simultaneous extraction of optical and thermal parameters and thickness values for multi-layered sound and artificial demineralized enamel lesions [7].

The aim of the present study was to evaluate the ability and efficacy of PTR-LUM to detect, longitudinally monitor and quantify the fluoride-mediated remineralization of artificial enamel demineralized lesions. Theoretical best fits of remineralized PTR amplitude and phase curves were used to extrapolate and predict the physical characteristics of the demineralized lesions prior to remineralization as well as follow the changes in opto-thermophysical properties as a function of time of exposure to the remineralizing solutions.

2. Materials and methods

2.1 Sample preparation

Forty erupted and visually sound human molars extracted by dental professionals for orthodontic or other surgical purposes were collected, debrided of all soft attached connective tissue and sterilized using gamma irradiation (4080 Gy) prior to use. The study protocol was approved by the University of Toronto Ethics Review Board (Protocol #25075). Individual samples were mounted on LEGO® blocks to allow for the precise realignment of samples on a micrometer-scale 3-axis precision stage during subsequent measurements. All samples were sealed in a chamber containing Petri dishes of distilled water to maintain ambient humidity conditions. Samples were maintained in the humid chamber at all times, excluding the time when measurements and treatments were being executed. Retaining the samples in the humid chamber maintained ambient conditions in a thermodynamically stable state and preserved sample hydration for the duration of the experiment. An acid-resistant nail varnish was applied to all surfaces of the teeth except a delimited 6×6 mm lingual/palatal enamel treatment window, which was exposed to the artificial demineralizing/remineralizing solutions and probed with the PTR-LUM system. All measurements were performed at room temperature and constant humidity in a laboratory-controlled environment.

2.2 Demineralization and remineralization treatments

Samples were randomly distributed into 4 treatment groups ($n = 10$/group). Group 1 was only demineralized. The remaining 3 treatment groups were subjected to a mineral solution with variations in fluoride content; either no fluoride (Group 2), low fluoride (1 ppm) (Group 3) or high fluoride (1000 ppm) (Group 4). Fluoride was added in the form of NaF. All demineralizing and remineralizing treatments were conducted at room temperature and in sealed experimental tubes.

2.2.1 Demineralization

Artificial smooth-surface enamel demineralization, simulating initial carious lesions, was induced using a well-characterized acidified gel system [8]. The demineralizing gel contained 0.1 M lactic acid gelled to a thick consistency with 6% hydroxyethyl cellulose (HEC) and adjusted to pH 4.5 by the addition of 0.1 M NaOH [9]. Samples were incubated in 30 mL of demineralizing gel and left unagitated for the duration of the treatment period. Samples were demineralized for a period of up to 10 days, with sample interruption for PTR-LUM measurements after 5 days and 10 days of acid exposure. Following demineralization, all samples were rinsed under running distilled water for 2 minutes in order to remove any residual adsorbed gel on the enamel surface. The teeth were dried in ambient air for 1 hour, followed by incubation in the humid chamber until PTR-LUM scans were executed. The same procedure was followed for PTR-LUM scans after 5 days of demineralization.

2.2.2 Remineralization

The remineralizing solution was formulated as per Amaechi and Higham [7], consisting of 0.03 g/L $MgCl_2 \cdot 6\,H_2O$, 0.121 g/L K_2HPO_4, 0.049 g/L KH_2PO_4,

0.625 g/L KCl, 3.85 g/L calcium lactate, 2.0 g/L methyl-*p*-hydroxybenzoate and 0.4 g/L sodium carboxymethylcellulose (CMC). The pH was adjusted to 7.2 using KOH. Individual experimental groups were exposed to the remineralizing solution for 4 weeks formulated with different concentrations of fluoride, 0 ppm, 1 ppm or 1000 ppm. The addition of CMC increased the viscosity of the remineralizing solution to a consistency comparable to natural saliva [10]. The remaining compounds provided the inorganic components required for the remineralization process. The main constituents of enamel mineral, calcium and phosphate, were added to the remineralizing solution in the form of calcium lactate and phosphate complexes, respectively [9]. Samples were inverted and immersed in 30 mL of solution, renewed every 5 days. Following individual treatments, samples were rinsed under running distilled water for 2 minutes and left to air dry for 1 hour. After drying, samples were placed in the humid chamber until PTR-LUM scans were performed.

2.3 PTR-LUM experimental setup and measurements

The PTR-LUM experimental set-up is shown in Figure 1. The laser light source was a semiconductor laser diode emitting at 659 nm (Mitsubishi ML101J27, Thorlabs, Newark, NJ, USA; optical power output = 130 mW, beam size ≈ 5.60 mm). A diode laser driver (LDC 210, Thorlabs, Newark, NJ, USA) triggered by the built-in function generator of the lock-in amplifier (SR830, Stanford Research Systems, Sunnyvale, CA, USA) modulated the laser current harmonically. The modulated infrared PTR signal from the tooth was collected and focused by two off-axis paraboloidal mirrors (Melles Griot 02POA017, Rhodium coated, Albuquerque, NM, USA) onto a Mercury Cadmium Telluride (MCT) detector (Judson Technologies J15D12, Montgomeryville, PA, USA; spectral range: 2 to 12 μm, peak detectivity $\approx 5 \times 10^{10}$ cm $Hz^{1/2}$ W^{-1} at ca. 12 μm) operating at cryogenic temperatures by means of a liquid-nitrogen cooling mechanism and with an active area of 1 mm^2. Before being sent to the lock-in amplifier, the PTR signal was amplified by a preamplifier (Judson Technologies PA-101, Montgomeryville, PA, USA). The collected modulated luminescence was focused onto a silicon photodiode with a coloured glass filter (Oriel 51345, cut-on wavelength: 715 nm) placed in front of the photodetector to block laser light reflected or scattered by the tooth. For monitoring the modulated luminescence signal, a second lock-in amplifier (SR850, Stanford Research Systems, Sunnyvale, CA, USA) was used. Both lock-in amplifiers were controlled by a computer via USB to RS-232 port connections.

Frequency scans measured PTR and LUM signals during a scan of laser beam modulation frequency from 1 Hz–1 kHz in the center of the delineated treatment window before and periodically during the acid treatment. The frequency range was segmented into 21 steps on a logarithmic scale by Labview-controlled computer software (National Instruments, Austin, TX, USA) to automatically increment frequencies sequentially. Twenty-four seconds of stabilization time was implemented following a change in frequency before data were recorded. For samples in group 1, PTR-LUM measurements were performed after 5 and 10 days of demineralization. For samples in groups 2–4 PTR-LUM measurements were carried out at day 5 and 10 of deminera-

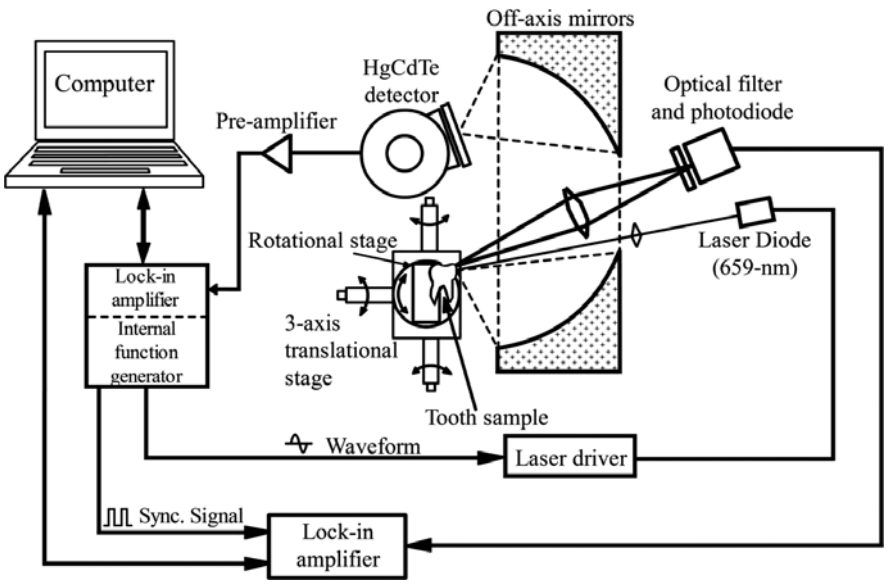

Figure 1 Schematic of the PTR-LUM experimental set-up.

lization and at day 2, 5, 10, 20 and 28 following exposure to the remineralizing solution. Standardized measurement conditions were implemented for all sample frequency scans during the course of treatment. Prior to PTR-LUM measurements, samples were removed from the humid chamber, air dried for 20 minutes, followed by a further 10 minutes with the sample placed under direct laser incidence for thermal stabilization. This standardized procedure was followed for all PTR-LUM scans and based on the earlier observation that changes in optical properties, observed as changes in luminescence intensity, and thermal properties, were negligible following 20 minute stabilization time, for experimentation lasting less than 1 hour [11]. The total drying time implemented in the present study was in-line with previous *in vitro* reports employing a 30 min [12] to 45 min [13] stabilizing period.

To obtain meaningful information from PTR frequency-scan data and remove any influence of instrumental effects, the experimentally measured signals were normalized against an opaque semi-infinite Glassy Carbon reference sample, as detailed in Hellen et al. [14].

2.4 Transverse microradiography (TMR) and image analysis

Following completion of all PTR-LUM measurements all samples were subjected to transverse microradiography (TMR) analysis to determine the mineral loss and depth of the artificially demineralized lesions. The samples were sectioned using a water-cooled diamond-coated wire saw model 3242 (Well, Le Locle, Switzerland), to produce a thin enamel slice approximately 100 μm from the lesion area. The slice, together with an aluminum step wedge (10 steps of 24.5 μm thickness), was microradiographed on type lA high resolution glass X-ray plates (IMTECH CA, USA) with a Phillips X-ray generator system equipped with a nickel filtered Cu-Kα target, producing monochromatic radiation of wavelength appropriate for hydroxyapatite (l84 Å). The plates were exposed for 10 minutes at 20 kV/10 mA, and processed. Processing consists of a 5 minute development in a developer (Kodak HR) and 15 min fixation in a Rapid-fixer (Kodak) before a final 30 minute wash period. After drying, the microradiographs were visualized using an optical microscope (Leica DMR, Microsystems, Wetzlar, Germany) linked via a CCTV camera (Sony, XC-75CE) to a personal computer. The enhanced image of the microradiograph was analyzed under standard conditions of light intensity and magnification and processed, along with data from the image of the step wedge, using the TMR software (TMRW version 2.0.27.2, Inspektor Research Inc., Amsterdam, Netherlands) [15] to quantify the lesion parameters of integrated mineral loss (vol% μm) and lesion depth (μm). The implementation of the latest dedicated TMR software package utilized a new algorithm developed to mathematically flatten curved tooth surfaces, by completing several scans for each microradiographed section. The mineral loss was computed as the difference in volume percent of mineral between sound and demineralized tissue integrated over the lesion depth. The mineral content plateau in deeper regions of the enamel section, representative of sound tissue, was preset at the 87 vol% level [15]. The lesion depth was determined as the distance from the measured sound enamel surface to the location in the lesion where mineral content was 95% of the sound enamel mineral volume. Lesion parameters were determined by averaging several scans over the distance of the thin section taken from the center of the treated area and corresponding to the irradiated beam size in PTR-LUM experimental measurements.

2.5 Theoretical model and multiparameter fitting of experimental curves

Experimental PTR amplitude and phase signals were fitted to the 3-layer coupled diffuse-photon-density-wave and thermal-wave theoretical model using the simplex downhill algorithm [16] initially applied by Matvienko et al. [17] and further advanced by Hellen et al. [14] for the investigation of multilayered sound and demineralized enamel. A detailed description of the theoretical model and the multiparameter fitting procedure used in the present study can be found in Hellen et al. [14]. Briefly, the model is based on the computational simulation of optical and thermal fluxes within each effective enamel layer considered in the analysis. The designation of "effective layers" was based on the sample treatments, where a 2 and 3-layer approximation was assumed for sound and de/remineralized enamel, respectively, and was borne out by TMR cross-sectional images [14]. In the present investigation, a 3-layer analysis was implemented in order to simulate the geometrical and histological configuration of initial demineralized and subsequently remineralized lesions (Figure 2). The justification of the 3-layer model was made using TMR cross-sectional images in this work and in Hellen et al. [14]. The fitting of the experimental PTR data to the theoretical model results in the extraction of multiple opto-thermophysical parameters for each effective layer. A select subset of all the parameters extracted from the theoretical multi-parameter fits of demineralized samples was found to be very reliable and changed consis-

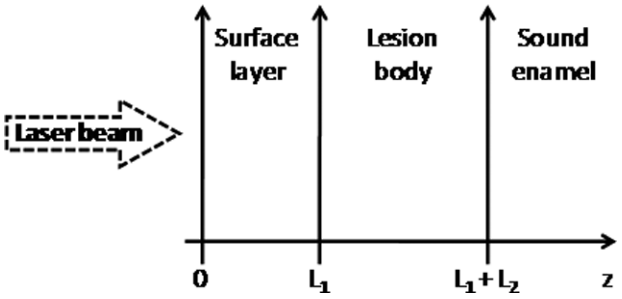

Figure 2 Schematic structure of effective layers used for fits of demineralized and remineralized enamel. L_1 = surface layer; L_2 = lesion body; sound enamel is assumed semi-infinite, $z > L_1 + L_2$.

tently with treatment time [18]. The subset includes the main optical and thermal transport properties (optical scattering and absorption coefficients, thermal conductivity and diffusivity) and layer thicknesses. They play a central role in the theory of dental PTR in terms of high signal sensitivity to their variation and form the basis of the present investigation.

Experimental PTR frequency-scan data, amplitude and phase, were fitted across the frequency range of 4 Hz–354 Hz. For remineralized samples, final PTR amplitude and phase curves at the conclusion of all treatments were initially fitted using layer thicknesses obtained from TMR mineral content profiles, by defining a maximum and minimum thickness of the surface layer (L_1) and lesion body (L_2). All other parameters were allowed to vary between the limit ranges defined by literature values [14]. From the fit of the final PTR curve, the TMR-measured thicknesses of layer 1 and 2 were fixed as the upper and lower limit, respectively, for fitting the final demineralized PTR curve. In this way, two treatment end points were defined in fitting the intermediate PTR curves during remineralization. The lower limit for layer 1 was set at 5 μm, which was the lower limit of the aprismatic surface layer for fitting sound enamel. This was done in order to account for large aprismatic layers that may decrease in thickness during the demineralization period. The upper limit for layer 2, the lesion body, was set as the difference between the depth at the sound enamel level (87 vol%) and the depth at the maximum thickness of the surface layer. Following the derivation of parameters corresponding to the 2 treatment end-points (the final demineralization treatment being one endpoint, and the final remineralization treatment, the other), thicknesses of both layers were fixed for fitting intermediate remineralization PTR curves. The major physically reasonable constraint in the theoretical fitting procedure was that intermediate thicknesses for layers 1 and 2 could not be larger than the final thicknesses calculated from the fitting of final PTR signals, which were based on TMR microradiographs.

2.6 Statistical analysis

Data obtained from TMR image analysis were analyzed statistically. Significant differences between demineralized and remineralized lesions in terms of lesion depth and mineral loss in the presence of variable fluoride concentrations were examined using ANOVA and post hoc Tukey's test at a significance level of $p < 0.05$. All statistical analysis was done using statistical analysis software (SPSS v. 14.0 for Windows, SPSS Inc., Chicago, IL).

3. Results

3.1 Microradiographic analysis

Average mineral loss and lesion depths of remineralization and demineralization treatment groups are presented in Table 1. Analysis of variance of the treatment groups with respect to mineral loss and lesion depth revealed no significant differences in mean mineral loss ($p > 0.05$), and a significant difference in mean lesion depth ($p < 0.05$). Post hoc statistical analysis (Tukey test) revealed a significant difference in mean lesion depth between all 3 remineralization groups relative to the demineralized control ($p < 0.05$). No significant differences were found between the 3 remineralization treatment groups with respect to mineral loss.

Table 1 Average mineral loss and lesion depth of remineralization and demineralization treatment groups. Means with different superscripted letters (a, b) are significantly different at $p < 0.05$.

Treatment Group	Mean mineral loss (vol% μm)	Mean lesion depth (μm)
Group 1: Demineralized	1247 ± 502	90 ± 12[a]
Group 2: No Fluoride	1055 ± 257	65 ± 7[b]
Group 3: Low Fluoride (1 ppm)	1087 ± 452	64 ± 11[b]
Group 4: High Fluoride (1000 ppm)	932 ± 373	60 ± 15[b]

3.2 Demineralization group

The PTR-LUM signals during the demineralization phase of the remineralized samples produced amplitude and phase signal trends consistent with the formation of artificial subsurface lesions [18]. Furthermore, the enhanced optical scattering coefficient and poorer thermophysical properties over the 10 day demineralization period were also consistent with the formation and progression of lesions as described in further detail in Hellen et al. [18].

3.3 Fluoride-free remineralization group

3.3.1 Microradiographs and mineral content depth profiles

An exemplary sample from the fluoride-free group (Figure 3) revealed a heavily mineralized superficial enamel layer, overlying the intact surface layer and body of the lesion (Figure 3B). This typical mineral volume distribution was the most frequently observed occurring in 80% of remineralized samples. Hypermineralized surface layers, with respect to the intact surface layer and lesion body, were present at mineral volume approaching sound enamel and higher than the mineral volume of the subadjacent intact surface layer. In these samples, mineral volume peaks occurred directly at the enamel surface and in microradiographic images displayed as thin radiopaque surface layers discernible from underlying mineral layers.

3.3.2 PTR-LUM frequency response

In order to enhance signal trends, PTR and LUM amplitude ratios and phase differences with respect to the final demineralized state of a sample representative of the fluoride-free treatment group are shown in Figure 3A. Amplitude ratios greater or less than unity indicate an increase or decrease in amplitude above or below the final demineralization curve, respectively, across the probed modulation

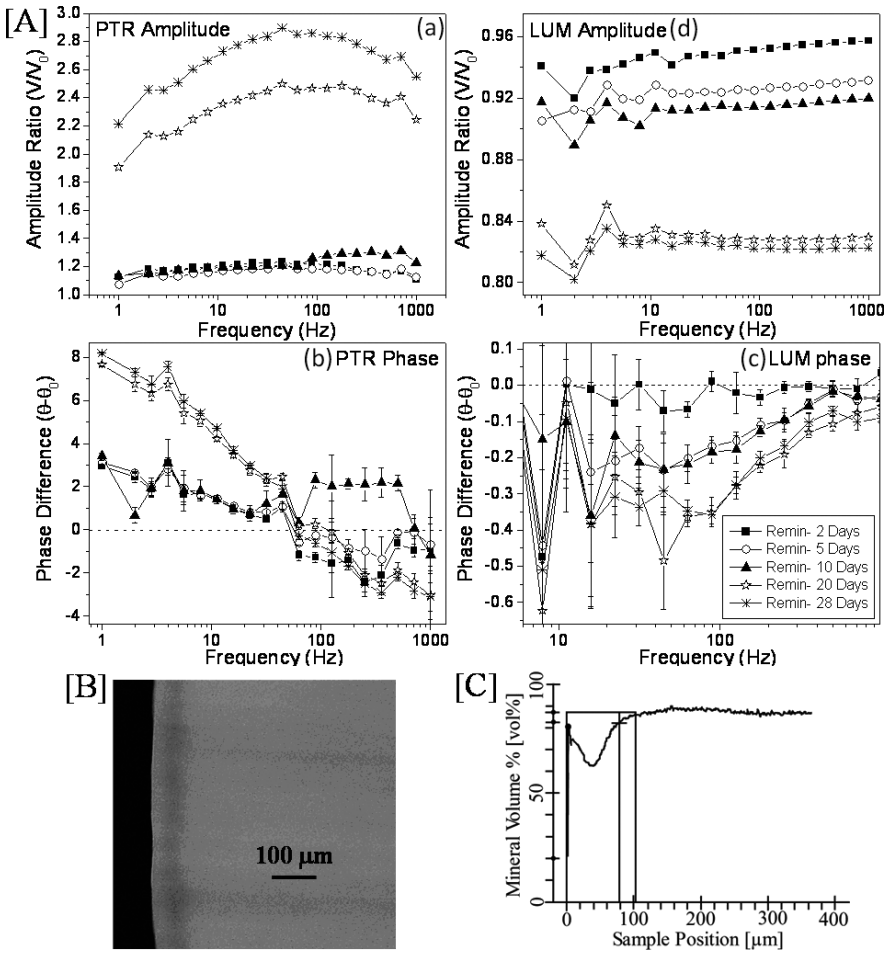

Figure 3 (**A**(a–d)) PTR-LUM amplitude ratios and phase differences with respect to the final demineralization state for a sample in the fluoride-free treatment group. Error bars, when not visible, are of the size of the symbols. The corresponding microradiograph and mineral volume profile is shown in (**B**) and (**C**), respectively. The solid vertical line in (**C**) indicates the sample depth at which mineral volume is at 87 vol% and the vertical line with the cross indicates the lesion depth at which mineral volume is 95% of the sound enamel mineral volume.

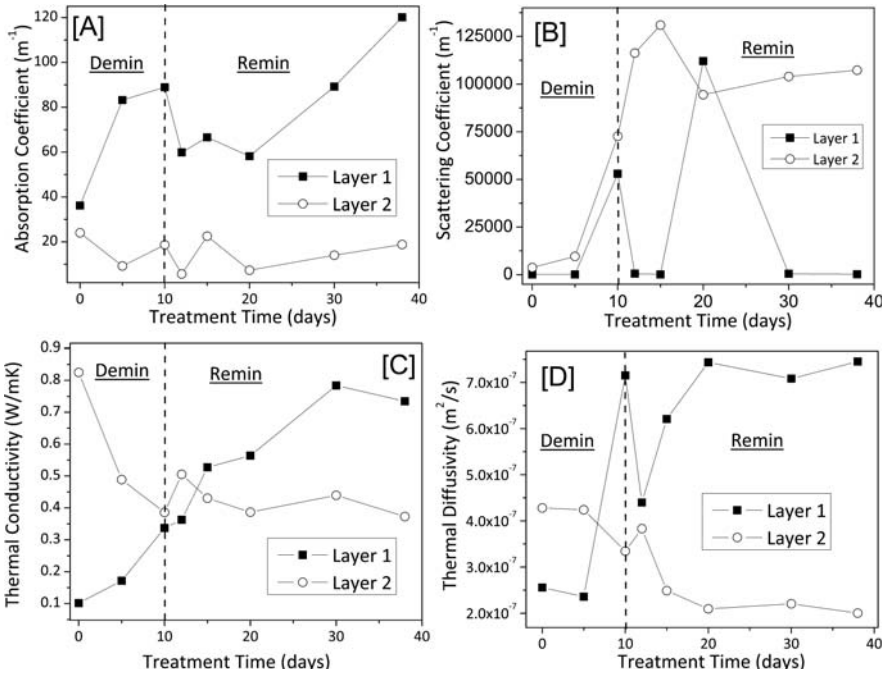

Figure 4 Change in optical and thermal properties over treatment time for a typical sample in the fluoride-free treatment group. (**A**) absorption coefficient, (**B**) scattering coefficient, (**C**) thermal conductivity and (**D**) thermal diffusivity. Vertical dashed lines separate demineralization and remineralization treatments. Layer 1 = surface layer; Layer 2 = lesion body.

frequency range. Positive and negative phase differences refer to smaller and larger phase lags, respectively. Following demineralization until the final remineralization treatment point there was a trend of increasing PTR amplitude across the entire frequency range and decreasing PTR phase lag, particularly at low modulation frequencies. The PTR amplitude shifted very slowly and mostly at high modulation frequencies (shallow depths) during the first 10 days of exposure to the mineralizing solution, however, following 10 days the curves rapidly and consistently increased in amplitude until the end of the exposure period. An increase in phase lag at high frequencies ($\geq$60 Hz) occurred at all treatment points except day 10, where a drastic and transient decrease was observed, consistent with the PTR amplitude increase.

LUM amplitude ratios, normalized with respect to the final demineralized curve, revealed relatively flat frequency dependence with vertical shifts in amplitude (Figure 3A(d)). LUM phases exhibited minima in the modulation frequency range 63–100 Hz. It is important to note that LUM trends were opposite to those of PTR, such that higher PTR signal amplitude correlated with lower LUM signal amplitude and vice versa. Decreases in LUM amplitude and phase minima, Figures 3A(c, d), occurred over the first 10 days. A further large increase in amplitude and phase after 20 days was followed by a smaller decrease at 28 days. These changes are consistent with the surface-dominated nature of dental fluorescence (luminescence). Comparisons with the PTR signal shifts, Figures 3A(a, b), show that the LUM signal can be valuable in corroborating surface structure changes as the cause of high-frequency variations of the depth-sensitive PTR signal. Figure 3B and all other TMR cross-sections further on, justifies the use of the 3-layer model in this work.

3.3.3 Theoretical analysis of fluoride-free remineralized samples

The opto-thermophysical depth profiles were constructed from the fitting of the 3-layer theory [7] to experimental PTR curves during demineralization and all remineralization treatment periods. The fitting procedure to PTR experimental data yielded excellent fits with small residuals for all samples in each remineralization treatment group, as was previously found for the theoretical fit of sound and demineralized enamel PTR data [14]. The change in optical parameters (absorption and scattering coefficients) and thermophysical parameters (diffusivity and conductivity) as a function of demineralization time (10 day) and subsequent remineralization (4 week) in the fluoride-free solution is shown in Figures 4A–D. At the onset of remineralization, a decrease in optical absorption coefficient of both layers demineralized for 10 days was followed by a linear increase in layer 1 until the end of the 4 week period, Figure 4A. The optical scattering coefficient within the lesion body continued to rise following the onset of remineralization, whereas in the surface layer an increase in the scattering coefficient, noted at the 10 day remineralization period, Figure 4B, was followed by a decrease, Figure 4B. The large lesion-

body scattering coefficient increases during the early remineralization phases and is clearly dominant over the much smaller and non-monotonic changes in the absorption coefficient and those in the much thinner surface layer. This is consistent with the smaller phase lag at high modulation frequencies and increase in slope of the amplitude ratio of the 10 day remineralized curve, Figures 3A(a, b). At the onset of remineralization, a large decrease in thermal diffusivity of the surface layer (Figure 4D) occurred with a small increase in the subsurface layer. Surface layer diffusivity increased over the remineralization period and saturated after 10 days. The diffusivity of the lesion body changed in a similar fashion, decreasing monotonically after the first two days of the 10-day remineralization and then saturating. Thermal conductivities (Figure 4C) exhibited similar trends to diffusivities as expected from the direct proportionality relationship between the two properties: that of the surface layer also increased with increasing remineralization time, but only small increases were observed in layer 2 after 5 days of remineralization.

3.4 Low fluoride (1 ppm) remineralization group

3.4.1 Microradiographs and mineral content depth profiles

An exemplary sample from the low fluoride group revealed a more discernible approximate 3-layer geometrical lesion structure, outlining a radiodense intact surface layer overlying the lesion body and followed by bulk sound enamel (Figure 5).

3.4.2 PTR-LUM frequency response

The PTR-LUM frequency response is shown in Figure 5A. An overall trend of increasing PTR amplitude across the entire modulation frequency range and decreasing phase lag at low frequencies from the final demineralization curve to the final reminer-

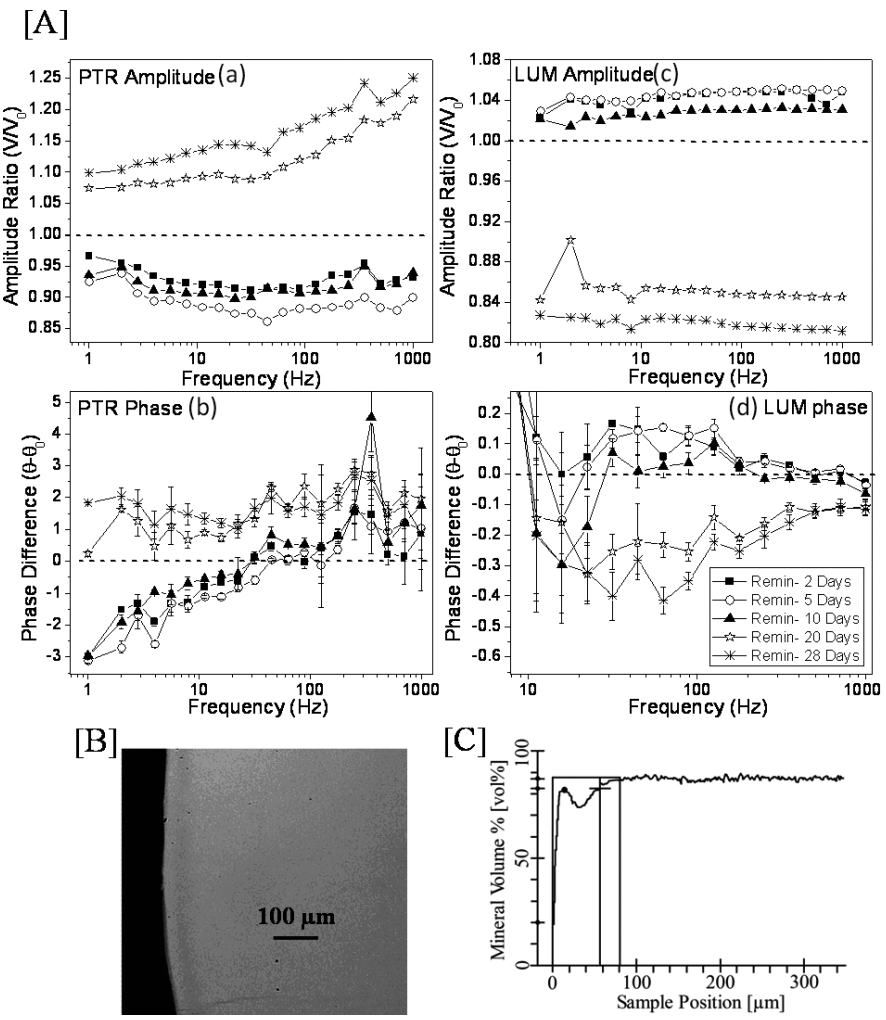

Figure 5 (**A**(a–d)) PTR-LUM amplitude ratios and phase differences with respect to the final demineralization state for a sample in the low-fluoride treatment group. Error bars, when not visible, are of the size of the symbols. The corresponding microradiograph and mineral volume profile is shown in (**B**) and (**C**), respectively. Vertical lines in (**C**) are similar to Figure 3.

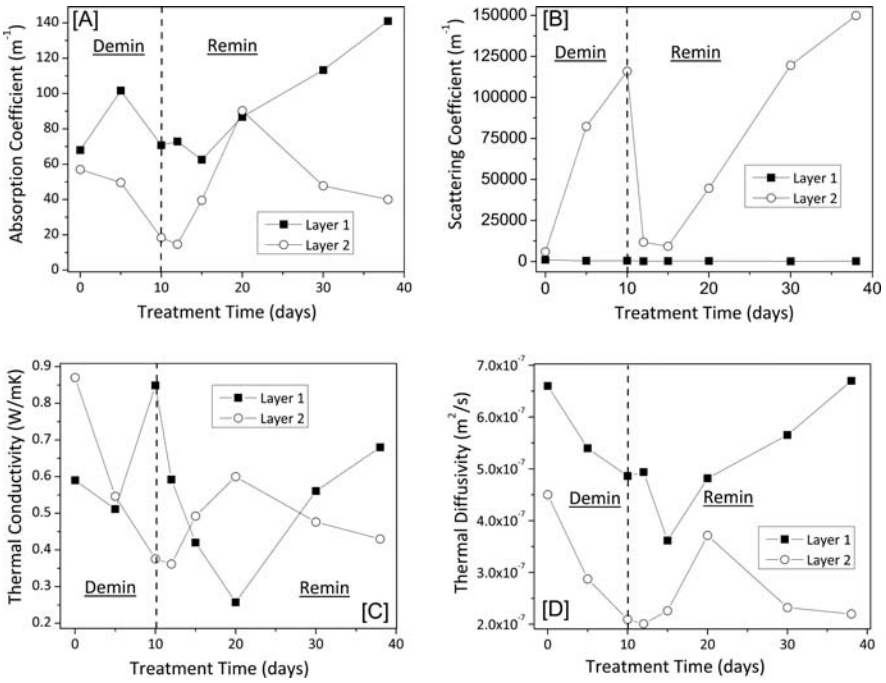

Figure 6 Change in optical and thermal properties over treatment time for a sample in the low-fluoride treatment group. (**A**) absorption coefficient, (**B**) scattering coefficient, (**C**) thermal conductivity and (**D**) thermal diffusivity. Vertical dashed lines separate demineralization and remineralization treatments. Layer 1 = surface layer; Layer 2 = lesion body.

alization curve is evident. However, marked differences are observed at earlier and later mineral solution exposure times. Large separation appears between measurements in the first 10 days and subsequent measurements at later periods. This behaviour is consistent with the fluoride-free groups of Figure 3. Furthermore, trends of increased slope in PTR amplitudes and phases for $f \geq 60$ Hz with a marked, approximately linear, increase in amplitude are evident at later remineralization times. Significant amplitude depression at the inception of the exposure period was noted and continued for 10 days. LUM amplitude and phase exhibit opposite trends to PTR and mirror changes in PTR: a reversal in direction occurred for the first 10 days of remineralization (Figure 5A(c, d)).

3.4.3 Theoretical analysis of low-fluoride remineralized samples

An increase in absorption coefficient of the lesion body occurred over the first 10 day remineralization period, Figure 6A, with an increase in the surface layer from day 20 until the end of the treatment period. A very substantial decrease in the scattering coefficient of the lesion body occurred over the first 5 days of remineralization, Figure 6B. From the 5 day remineralization period onward the lesion-body scattering coefficient began to rise steeply and increased above the final demineralized state at the 30–38 day overall treatment period. The scattering coefficient of the surface layer was insignificant compared to the absolute value and dominant changes of that of layer 2. At the onset of remineralization, an increase in the thermophysical properties (conductivity and diffusivity) of the lesion body is noted over the first 10 days, Figure 6C, D. They both begin to decrease at prolonged treatment times, consistent with the PTR amplitude and phase frequency response, Figures 5A(a, b). The improvement in the thermal conductivity and diffusivity of the lesion body over the first 10 days is in contrast to steep decreases in the conductivity and diffusivity of the surface layer, Figures 6C, D. After 20–28 days of remineralization increases in the thermophysical properties of the surface layer are evident. In summary, the thermophysical properties of the surface layer increased after 10–20 days of remineralization, Figure 6D.

3.5 High fluoride (1000 ppm) remineralization group

3.5.1 Microradiographs and mineral content depth profiles

A sample from the high fluoride group showed a hypomineralized layer above the intact surface layer which reached a maximum mineral volume at a depth below the enamel surface (≈14 μm). Typical results are shown in Figure 7. Surface hypomineralization was evident in 70% of the high fluoride group. Poorer distinction between the intact surface

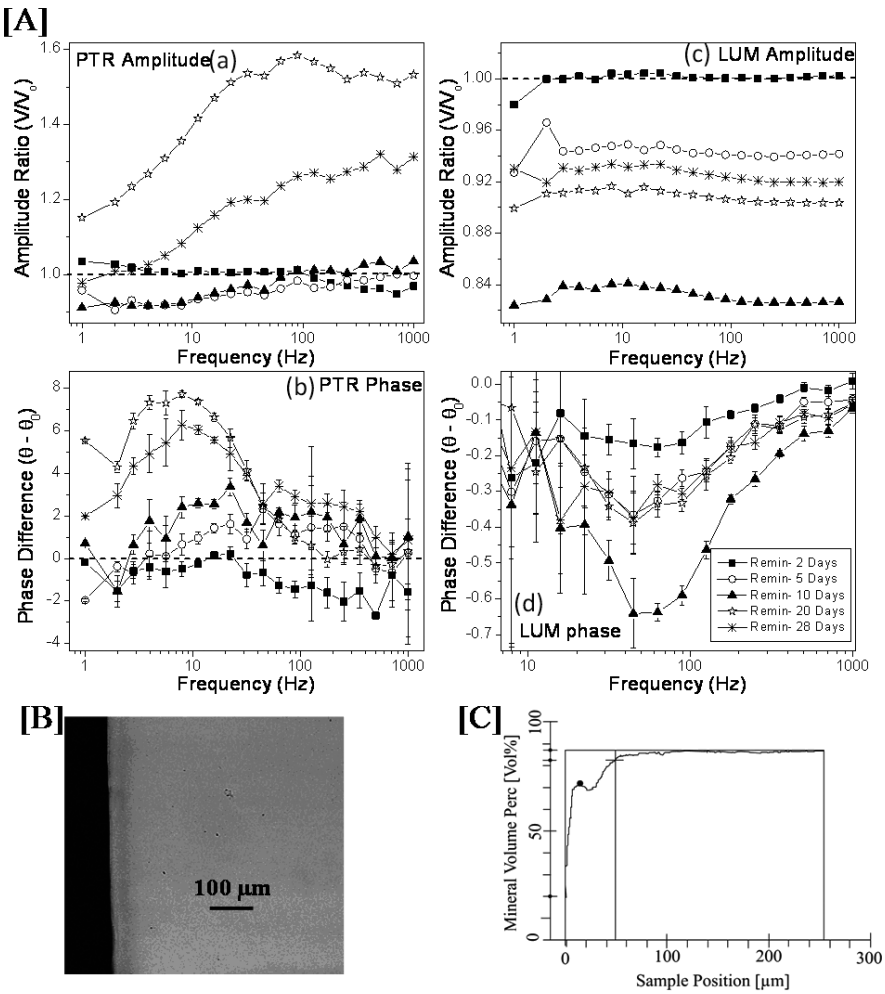

Figure 7 (**A**(a–d)) PTR-LUM amplitude ratios and phase differences with respect to the final demineralization state for a sample in the high-fluoride treatment group. Error bars, when not visible, are of the size of the symbols. The corresponding microradiograph and mineral volume profile is shown in (**B**) and (**C**), respectively. Vertical lines in (**C**) are similar to Figure 3.

layer and the subsurface lesion was due to reduced subsurface radiolucency.

3.5.2 PTR-LUM frequency response

PTR-LUM frequency responses for a sample from the high fluoride group are presented in Figure 7A. A decrease in low-frequency amplitude up to the 10 day exposure period is evident. Onward from the 10 day exposure period a substantial increase in PTR amplitude across all modulation frequencies and decrease in PTR phase lag at low modulation frequencies occurs. The low frequency PTR phase pattern is accentuated with increasing exposure time: a smaller phase lag and more pronounced curvature of the phase maxima. A trend consistent among all samples remineralized in the presence of high fluoride concentrations is the decrease in PTR amplitude across the entire modulation frequency range from the 20 day to the 28 day exposure period. This occurred with a concomitant increase in phase lag at low modulation frequencies.

LUM amplitude and phase signals do not exhibit trends consistent with treatment time; however, they reflect changes in PTR amplitude at high frequency (near-surface region, Figure 7A(a)). The larger PTR amplitude at high frequencies correlates with the lower LUM amplitude and vice versa. The small change in amplitude is accompanied by a decrease in phase at 2 days of remineralization. Marked reduction in LUM amplitude occurs after 5 and 10 days of remineralization in both samples. This is followed by a large increase in amplitude and phase at 20 days of remineralization, which continued to increase at day 28.

3.5.3 Theoretical analysis of high-fluoride remineralized samples

Optical and thermal properties derived from the PTR frequency response of the high fluoride sample are shown in Figure 8. An increase in the scattering coefficient of the lesion body after 2 days of remineralization rapidly declined at prolonged exposure

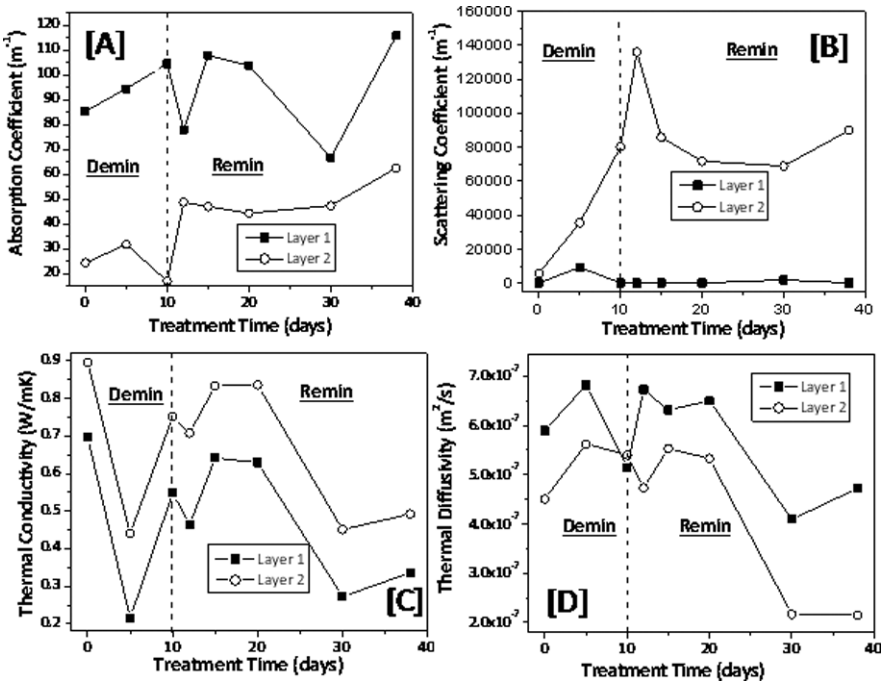

Figure 8 Change in optical and thermal properties over treatment time for a sample in the high-fluoride treatment group. (**A**) absorption coefficient, (**B**) scattering coefficient, (**C**) thermal conductivity and (**D**) thermal diffusivity. Vertical dashed lines separate demineralization and remineralization treatments. Layer 1 = surface layer; Layer 2 = lesion body.

times, Figure 8B. A slight reversal in the scattering coefficient led to an increase at the 28 day remineralization period. Changes in the scattering coefficient of the surface layer are small compared to the dominant changes in the lesion body. Remineralization enhanced the thermophysical properties of both layers over the 10 day remineralization period. At longer exposure periods to the fluoride solution, a large decrease in both thermal conductivity, Figure 8C, and thermal diffusivity, Figure 8D, was observed.

3.6 Theoretical analysis of layer thicknesses

Layer thicknesses were extracted from the theoretical model for the exemplary samples of each remineralization treatment group. The changes in thickness of the surface layer (layer 1) and lesion body (layer 2) for the fluoride-free, low-fluoride and high-fluoride treatment groups are displayed in Figure 9. In all 3 treatment groups, a steep increase in the thickness of the lesion body occurred over the 10 day demineralization period. At the onset of remineralization in all 3 groups, this was followed by a significant decrease in the thickness of the lesion, the rate of which was greatest in the high-fluoride group (Figure 9C), followed by the low-fluoride group (Figure 9B) and the fluoride-free group (Figure 9A). In all 3 samples, the largest reduction in the thickness of the lesion body occurred over the first 10 days of remineralization with little change in thickness thereafter. In the fluoride-free and low-fluoride group, the decrease in the thickness of the

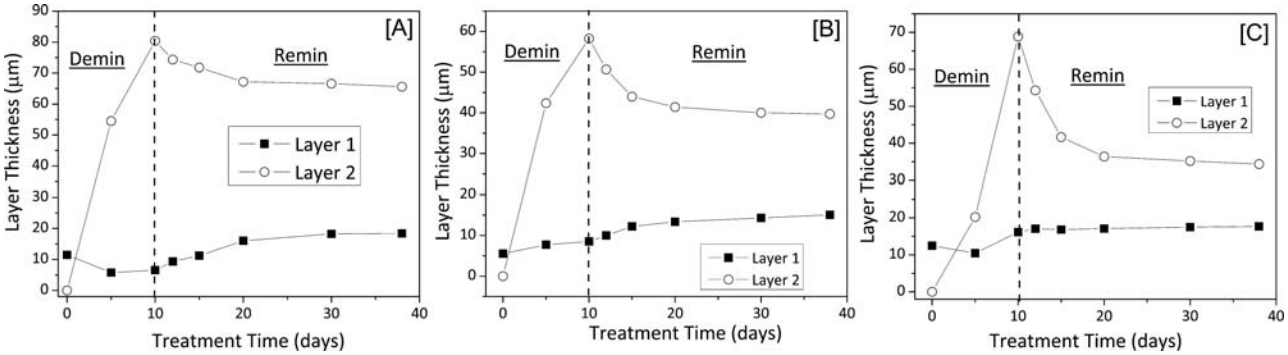

Figure 9 Change in layer thicknesses with treatment time for representative samples from the fluoride-free treatment group (**A**), low-fluoride treatment group (**B**) and high-fluoride treatment group (**C**). The vertical dashed line separates de- and remineralization treatments. Layer 1 = surface layer; Layer 2 = lesion body.

lesion body occurred with a concomitant increase in thickness of the surface layer. A smaller thickness increase was observed in the high-fluoride group over the 4 week remineralization period.

4. Discussion

All three remineralization treatment groups exhibited reductions in lesion depth compared to the demineralization control group (ANOVA, $p < 0.05$), illustrating significant remineralization induced by all three mineral solutions (Table 1). No significant differences in mineral loss were observed between the four treatment groups ($p > 0.05$). The large variance in mineral loss of the demineralized control group may have precluded the identification of reduction in mineral loss following remineralization. Large variation in the extent of demineralization and remineralization was noted elsewhere [19] and attributed to small differences in structure and mineral content between and within individual samples and sections. In terms of demineralization, the consistent trends of enhanced scattering coefficients and poorer thermophysical properties in the lesion body [18], were evident in the demineralized portion of the remineralized samples (Figures 4, 6 and 8). However, slight deviations from these trends were observed in Figures 8C, D and were attributed to the variance in lesion formation, in particular due to the utilization of intact teeth for artificial lesion formation which maintain higher intrinsic fluoride levels in the outermost enamel [20]. Changes in LUM signals during lesion progression were previously explained on the basis of enhanced light scattering properties of demineralized enamel and the channelling of radiative to non-radiative energy sources caused by the loss of inorganic structure [18].

Differences in PTR amplitude and phase were noted between earlier and later treatment times within all three treatment groups. Specifically, after the 10 day exposure period, amplitudes significantly increased and phase lags decreased monotonically until the end of the treatment period. This behaviour may be related to the kinetics of the process of remineralization, the rate of which depends on the availability of growth sites within a lesion and porosity of the intact surface layer [2]. The remineralization process has been known to proceed via three main routes: the restoration of partially demineralized crystallites, growth of residual crystals and *de novo* crystal formation [21]. Early on, following exposure of the demineralized lesion to supersaturated mineralizing solutions enamel porosity is high and the surface area available for crystal growth is large, resulting in precipitation on residual enamel crystallites [22]. However, once the pores in the surface layer become occluded with precipitated mineral, diffusion fluxes across the surface layer are retarded and remineralization of the inner lesion body is inhibited or reduced [23]. Rapid initial remineralization followed by slower rates at prolonged treatment times has been documented in the literature for decades. Johansson [24] found rapid remineralization over the first 24 hours, a reduced rate over 48 hours and no further change thereafter for 3 weeks. When fluoride was added to an artificial remineralizing solution at levels between 1–10 ppm, maximum changes were found to occur over a 10 day period [25]. Lastly, Al-Khateeb et al. [26] found that remineralization varied within the first week between the different treatment groups, with fluoride enhancing the process; however a plateau was reached thereafter. In a recent study implementing a similar artificial remineralizing solution, preferential initial mineralization occurred in deeper layers after 1 day of exposure, whereas after one week, enhanced mineralization was noted in the outermost mineralized layers [27].

During prolonged treatment times in all three mineralizing solutions (i.e. after 10 days), PTR amplitude and phase trends reversed direction resulting in a monotonic increase in amplitude with a smaller phase lag (Figures 3, 5 and 7). This may be attributed to the random orientation of deposited crystals as well as *de novo* mineral precipitation within the surface layer and lesion body, particularly within the interprismatic regions, a function of the lower specific surface area of the crystalline mineral phase [28]. An amorphous mineral phase would generate additional scattering centers through the larger number of crystal grain boundaries effectively increasing the scattering coefficient and creating poorer thermal properties as the density increases, both trends which were observed in the theoretical fittings (Figures 4B, C, D and 6B, C, D). Furthermore, a decrease in thermal properties at the final demineralization point or during the first 2 days of remineralization (Figures 4C, D; 6C, D; and 8C, D), was followed by a transient increase, and a further decrease at prolonged treatment times, an effect likened to competing thermal processes during the remineralization period. Higher absorption coefficients calculated after the 10 day remineralization period in the fluoride-free, Figure 4A, and low fluoride group, Figure 6A, may substantiate the proposed amorphous mineral precipitation, and has been documented in an earlier study [29]. At later remineralization times in the fluoride-free and low fluoride groups, a greater thermal mismatch was evident between the surface layer and subsurface layer (Figures 4C, D and 6C, D). As the surface layer becomes a better thermal conductor and diffuser, thermal energy will propagate rapidly toward the $(L_1 + L_2)$ interface (Figure 2). However, the poor subsurface

layer properties generate significant impedance to thermal fluxes and as a result, thermal energy will accumulate at the boundary. Effective confinement of the thermal-wave centroid will then occur within the surface layer thereby resulting in the observed increase in amplitude and smaller phase lag as the optical-to-thermal conversion process moves closer to the enamel surface. This may suggest an amplification of the dominant surface reaction whereby the effects of the underlying enamel at later remineralization times are concealed. Furthermore, this may imply that once the surface layer reaches a critical thickness its properties dominate the thermal response at the expense of the underlying enamel, which may require lower frequencies (longer thermal wavelengths) to probe deeper regions. The observed surface deposited mineral which was most prevalent in the fluoride-free group, Figures 3B, C, may chemically amount to a diffusion-barrier generating an impedance of inorganic mineral ion diffusion into deeper layers, while at the same time driving the thermal-wave centroid closer to the enamel surface, apparent in the increasing amplitude and smaller phase lag, Figures 3A(a, b). In all samples exhibiting this higher mineral volume in the most superficial part of the lesion (Figure 3C) resulted in the characteristic decreases in phase lag (or phase peaks) at high modulation frequencies (Figure 3A(b)). Not only did the presence of the surface mineralized layer correlate with the appearance of a smaller phase lag at high frequencies but also it correlated with the theoretical calculation of a higher scattering coefficient in the surface layer, Figure 4B. Larger absorption coefficients at later exposure periods in the surface layer (layer 1) may further support surface dominated reactions as the major contributor to the PTR signal, Figures 4A and Figure 6A. This is consistent with a recent PS-OCT study on the artificial remineralization of enamel where a highly scattering apatitic layer above the existing lesion surface was observed after 20 days of remineralization [30]. Therefore, changes in the PTR frequency response could be related to changes in the histological appearance of the lesion and further may be useful in determining lesion activity. On the other hand, the LUM channel did not exhibit a similar sensitivity during the remineralization period, Figure 3A(d). The high frequency of occurrence of the surface mineralized layer in the fluoride-free group (80%) compared to the low fluoride (40%) and high fluoride (30%) group provides additional support to the fluoride-enhanced deposition of mineral initially in deeper layers without preferential mineralization of the outer surface.

Although there were no significant differences between the remineralization treatment groups in terms of mineral loss and lesion depth, thicknesses derived from the theoretical fittings pointed toward preferential remineralization of subsurface layers in the presence of fluoride (Figure 9). It follows that in the absence of fluoride, surface mineral deposition was dominant, which was evident in the increase in layer 1 (surface layer) thickness relative to layer 2 (lesion body) (Figure 9A). In the presence of high fluoride levels, the theory-derived thicknesses indicated that subsurface remineralization was the dominant process. The low-fluoride group maintained intermediate characteristics between the fluoride-free and high-fluoride groups, with rapid decreases in the lesion body thickness and increases in surface layer thickness. The contrasting behaviours in the presence vs. absence of fluoride support the fluoride-enhancing effect on the remineralization process described in earlier Ref. [31]. In the presence of low-fluoride levels, a rapid decrease in amplitude across the entire modulation frequency range and increase in phase lag at low frequency was observed for the first 10 days (Figure 5). A set of derived optical and thermal parameters for the surface layer and lesion body presented different trends as a function of treatment time (Figure 6). The initial rapid decrease in amplitude and increase in phase lag, Figure 5A, may be attributed to the large decrease in scattering coefficient of the lesion body, Figure 6B. The decrease in optical scattering coefficient may be related to the restoration of enamel crystallinity within the lesion body, thereby reducing the acid-induced porosity. At the crystalline level, this is consistent with the previously described mechanisms of enamel remineralization, where the restoration of pre-existing, residual enamel crystals partially dissolved during the demineralization process and the growth of surviving crystals is the favoured process [21]. Mineral deposition was found to account for changes in the optical properties using polarized light microscopy by the deposition of suitably oriented OHAp crystallites [32]. Crystal growth is further enhanced by the presence of low levels of fluoride in solution (1 ppm) due to the elevated driving force for mineral deposition, in the form of FAP or F-OHAp, in the surface and subsurface regions [23]. Low incident-photon scattering coefficient, Figure 6B, combined with the improvement of the thermal properties of the lesion body, Figure 6C, D, up to 10 days following remineralization treatment, may support the enhanced crystallinity of the lesion body, driving the thermal centroid deeper into the enamel. This trend is supported by the abovementioned trends in PTR frequency response as a decrease in PTR amplitude across the entire modulation frequency range and increase in phase lag at lower modulation frequencies, Figure 5A(a, b). The validity of the proposed mechanism is further supported by the observation that LUM amplitude and phase for the sample exposed to the low fluoride solution were strongly correlated with the derived scattering coefficient. The rapid decrease in scattering coefficients of the lesion body,

Figure 6B, a result of enhanced crystallinity, would induce longer optical path lengths and greater luminescence generation as is seen in the larger LUM amplitude, Figure 5A(c). The observed increase in the absorption coefficient, Figure 6A, would tend to have the opposite effect, decreasing optical path lengths, however, given the magnitude of change in the scattering coefficient compared to the absorption coefficient it is clear that the scattering depression is dominant. LUM signals from the fluoride-free sample, Figure 3A(c), also exhibit trends correlated with the scattering coefficients, Figure 4B. However, this is not the case in the high fluoride group, Figures 7A and 8B. It is important to note that remineralization of demineralized lesions may not result in fluorescence gain equal to that lost from the enamel during lesion formation [33]. This is most likely attributed to the heterogeneity in the demineralized and remineralized enamel structures, which will induce scattering properties unique to individual samples, a function of the deposited mineral phase.

PTR-LUM frequency responses and theoretical fittings of the high-fluoride sample displayed trends that deviated from the low-fluoride and fluoride-free samples. In the high-fluoride sample, a decrease in amplitude following the first 10 days of remineralization, predominately at low modulation frequencies, was accompanied by a near-monotonic decrease in phase lag across the same frequency range, Figure 7A(b). This may suggest significant mineral deposition within the lesion body such that the regression in the thickness of the subsurface layer progresses from the advancing front of the lesion toward the surface layer. The higher fluoride concentrations would be expected to diffuse rapidly into deeper areas, due to higher concentration-gradient-induced driving forces, within the porous demineralized enamel thereby increasing total fluoride within the lesion to enhance mineral accretion. After 10 days of exposure to the high fluoride solution a marked reduction in the thermal properties of both layers was evident, Figure 8C, D. This was accompanied by an increase in the absorption, Figure 8A, and scattering coefficients, Figure 8B, which was expected since an opaque and chalky macroscopic appearance of enamel was observed after the 4-week immersion in the high fluoride solution. The chemical behaviour in the presence of high fluoride, manifested as a surface hypomineralization, is supported by the minimal change in PTR-derived thickness of the surface layer thickness over the remineralization period, Figure 9C. Furthermore, the poorer thermal properties generated at prolonged remineralization times may reflect the formation or growth of a surface precipitate, possibly a CaF_2-like layer (Figure 8C, D). If a precipitate was formed at the enamel surface following fluoride exposure, the level of integration of this layer with the underlying enamel could not be determined from microradiographic analysis.

5. Summary and conclusions

As a non-invasive, non-destructive technique, the combination of PTR and LUM along with the applied theoretical photothermal model provides four distinct signal channels along with a comprehensive theoretical formalism to yield quantitative information regarding lesion severity and the progression or regression of lesion severity as a function of treatment time. Multi-parameter fits of PTR experimental data revealed a marked increase in optical scattering coefficients and the generation of poorer thermophysical properties during demineralization, consistent with crystalline disintegration and subsurface lesion formation. Trends in PTR signals and opto-thermophysical parameters during the remineralization phase indicated a multi-factorial and complex lesion repair process. This was considered as interplay between shifting thermal centroids, as mineral gains in surface and subsurface regions alter the opto-thermophysical properties of the effective layers as a function of remineralization time. The theoretical model pointed to a fluoride-enhanced remineralization of the lesion body, however, no statistically significant differences in TMR defined mineral loss and lesion depth were noted between the remineralization treatment groups. The promising results from the present investigation place the quantitative PTR and LUM technique at the forefront of non-destructive caries evaluation *in vitro*, above existing purely optical methods, in terms of the total information extracted from the generated signals. In light of the results of the present study, PTR-LUM signals and the theoretical formalism applied to PTR amplitude and phase to derive opto-thermophysical properties proved to be efficacious in measuring and quantifying mineralized layers generated during de- and remineralization processes.

Acknowledgements AM acknowledges funding from the Ministry of Research and Innovation (MRI), the Ontario Premier's Discovery Award, the Canadian Foundation for Innovation & Ontario Research Fund (CFI-ORF) and the Canada Research Chairs Program, as well as the Natural Sciences and Engineering Research Council of Canada (NSERC) through a Discovery Grant. The authors would also like to acknowledge Dr. Stephen Abrams of Quantum Dental Technologies for his input and valuable discussions.

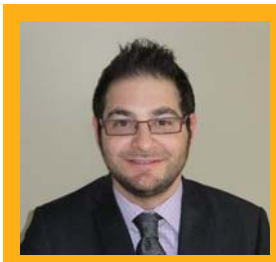

Adam Hellen completed his M.Sc. in the Faculty of Dentistry at the University of Toronto. This research paper emanates from his thesis work which focused on the ability of photothermal radiometry and modulated luminescence (PTR-LUM) to detect, longitudinally monitor and quantify simulated enamel demineralization/remineralization. He developed a theoretical model based on the photothermal radiometric signal to estimate lesion depths and optical/thermal properties. He is currently the Director of Research and Development for Quantum Dental Technologies, Inc., the developer of a clinical caries detection system based on PTR-LUM technology.

Andreas Mandelis is a Full Professor of Mechanical and Industrial Engineering; Electrical and Computer Engineering; and the Institute of Biomaterials and Biomedical Engineering, University of Toronto. He is also the CTO of Quantum Dental Technologies, Inc., Toronto, ON, Canada and President and CTO of Diffusion-Wave Diagnostic Technologies, Inc., Toronto. His scientific and technical research interests span all aspects of the physics, mathematics, instrumental implementation and experimental applications of novel laser-based diffusion-wave analytical inspection and monitoring techniques, high-precision measurement methodologies, environmental sensor device development, analytical, non-destructive and spectroscopic methodologies, signal processing physics and measurement science, and imaging techniques for industrial and health sector applications.

Yoav Finer completed his Ph.D. in Biomaterials and Biomedical Engineering and specialty training in Prosthodontics at the University of Toronto. He is an associate professor and director of the undergraduate Biomaterials Programmes and the Biomaterials Theme coordinators to the Dental Research Institute at the Faculty of Dentistry, University of Toronto. His main research activities include the development of biomaterials and techniques for implant supported prostheses, as well as composite resin biodegradation, bacterial role and host-biomaterial interactions. His research has been supported by the Canadian Institutes of Health Research (CIHR) and National Institutes of Health (NIH).

Bennett Amaechi is an Associate Professor and Director of Cariology in the Department of Comprehensive Dentistry at the University of Texas Health Science Center at San Antonio, USA. His main area of expertise is prosthetic dentistry, cariology, clinical preventive dentistry, dental erosion, caries detection, diagnosis and management with particular emphasis on Caries Management by Risk Assessment.

References

[1] L. C. Chow and G. L. Vogel, J. Opt. Dent. **6**, 27–38 (2001).
[2] J. M. ten Cate, J. Dent. Res. **69**, 614–619 (1990).
[3] B. T. Amaechi and S. M. Higham, J. Biomed. Opt. **7**, 7–13 (2002).
[4] R. S. Jones, C. L. Darling, J. D. B. Featherstone, and D. Fried, J. Biomed. Opt. **11**, 014016 (2006).
[5] O. Minet, K. Dörschel, and G. Muller, Laser Appl. Landolt–Börnstein **8**, 279–310 (2006).
[6] R. J. Jeon, A. Mandelis, V. Sanchez, and S. H. Abrams, J. Biomed. Opt. **9**, 804–819 (2004).
[7] A. Matvienko, A. Mandelis, and S. H. Abrams, Appl. Opt. **48**, 3193–3204 (2009).
[8] J. Arends and J. Schuthof, J. Biol. Buccale **8**, 175–81 (1980).
[9] B. T. Amaechi, S. M. Higham, and W. M. Edgar, Arch. Oral Biol. **43**, 619–628 (1998).
[10] B. T. Amaechi and S. M. Higham, Arch. Oral Biol. **46**, 697–703 (2001).
[11] B. Angmar-Mänsson, S. Al-Khateeb, and S. Tranaeus, Proc. 4th Annual Indiana Conf. on Early Detection of Dental Caries II, 203–217 (2000).
[12] I. A. Pretty, A. F. Hall, P. W. Smith, W. M. Edgar, and S. M. Higham, Br. Dent. J. **193**, 105–109 (2002).
[13] X. Z. Zhang, P. Anderson, S. E. P. Dowker, and J. C. Elliott, Caries Res. **34**, 164–174 (2000).
[14] A. Hellen, A. Matvienko, A. Mandelis, Y. Finer, and B. T. Amaechi, Appl. Opt. **49**, 6938–6951 (2010).
[15] E. de Josselin de Jong, A. H. I. M. Linden, and J. J. ten Bosch, Phys. Med. Biol. **32**, 1209–1220 (1987).
[16] W. H. Press, B. P. Flannery, S. A. Teukolsky, and W. T. Vetterling. Cambridge University Press (1988).

[17] A. Matvienko, A. Mandelis, A. Hellen, R. J. Jeon, S. H. Abrams, and B. T. Amaechi, Proc. SPIE. **7166**, 71660C (2009).
[18] A. Hellen, A. Mandelis, Y. Finer, and B. T. Amaechi, J. Biomed. Opt., Accepted for publication (2011).
[19] X. J. Gao, J. C. Elliott, P. Anderson, and G. R. Davis, J. Chem. Soc. Faraday Trans. **89**, 2907–2912 (1993).
[20] J. Weatherell, C. Robinson, and A. S. Hallsworth. J. Dent. Res. **53**, 180–192 (1974).
[21] T. Yanagisawa and Y. Miake, J. Electron Microsc. **52**, 605–613 (2003).
[22] T. T. Thuy, H. Nakagaki, K. Kato, P. A. Hung, J. Inukai, S. Tsuboi, H. Nakagaki, M. N. Hirose, S. Igarashi, and C. Robinson, Arch. Oral Biol. **53**, 1017–1022 (2008).
[23] L. M. Silverstone, J. S. Wefel, B. F. Zimmerman, B. H. Clarkson, and M. J. Featherstone, Caries Res. **15**, 138–157 (1981).
[24] B. Johansson, J. Dent. Res. **44**, 64–70 (1965).
[25] L. M. Silverstone, Caries Res. **11**, 59–84 (1977).
[26] S. Al-Khateeb, R. Exterkate, B. Angmar-Månsson, and B. ten Cate, Acta. Odont. Scand. **58**, 31–36 (2000); S. Al-Khateeb, R. A. M. Exterkate, E. de Josselin de Jong, B. Angmar-Månsson, and J. M. ten Cate, Caries Res. **36**, 25–30 (2002).
[27] R. Tanaka, Y. Shibata, A. Manabe, and T. Miyazaki, PLoS. ONE. **4**, e5986 (2009).
[28] M. Yonese, J. L. Fox, N. Nambu, J. J. Hefferren, and W. I. Higuchi, J. Pharm. Sci. **70**, 904–907 (1981).
[29] D. J. Krutchkoff and N. H. Rowe, J. Dent. Res. **50**, 1621–1625 (1971).
[30] A. M. Can, C. L. Darling, and D. Fried, Proc. SPIE. **6843**, 68430T (2008).
[31] J. M. ten Cate and J. Arends, Caries Res. **11**, 277–286 (1977).
[32] L. M. Silverstone and D. F. Poole. J. Dent. Res. **48**, 766–770 (1969).
[33] E. de Josselin de Jong, S. Higham, P. W. Smith, C. J. van Daelen, and M. H. van der Veen, J. Appl. Phys. **105**, 102031 (2009).